

**Helicity-Correlated Systematics for SLAC Experiment E158\***

P. A. Mastromarino  
California Institute of Technology, Pasadena, CA 91125

T. B. Humensky  
Princeton University, Princeton, NJ 08544

K. Bega, E. W. Hughes, G. M. Jones  
California Institute of Technology, Pasadena, CA 91125

D. Relyea  
Princeton University, Princeton, NJ 08544

P. L. Anthony, A. Brachmann, J. Clendenin, F.-J. Decker, T. Fieguth, S. Rock,  
O. Saxton, Z. Szalata, J. Turner, M. Woods  
Stanford Linear Accelerator Center, Stanford University, Stanford, CA 94309

C. Arroyo, K. S. Kumar  
University of Massachusetts, Amherst, MA 01003

G. D. Cates  
University of Virginia, Charlottesville, VA 22904

Yu. Kolomensky  
University of California, Berkeley, CA 94720

**Abstract**

Experiment E158 at SLAC will make the first measurement of parity violation in Møller scattering. The left-right cross-section asymmetry in the elastic scattering of a 45 GeV polarized electron beam with unpolarized electrons in a liquid hydrogen target will be measured to an accuracy of better than  $10^{-8}$ , with the expected Standard Model asymmetry being approximately  $10^{-7}$ . Because helicity-correlated (left-right) charge and position asymmetries in the electron beam can give rise to systematic errors in the measurement, great care must be given to beam monitoring and control. We have developed beam current monitors that measure the charge per pulse at the  $3 \times 10^{-5}$  level and RF cavity beam position monitors that measure the position per pulse to  $1 \mu\text{m}$ , which should allow precisions of 1 ppb and 1 nm for the final integrated charge and position asymmetries, respectively. In addition, since most helicity-correlated systematics in the electron beam can be traced back to the laser that drives the photoemission from the GaAs source cathode, we first use careful control of laser beam polarization, point-to-point imaging, and other techniques to minimize systematics. We also provide the capability of modulating in a helicity-correlated way the laser beam's intensity and position as it strikes the photocathode, allowing the implementation of active feedbacks to ensure that the average charge and position asymmetries integrate close to zero over the course of the experiment. We present this system of precision beam monitoring and control and report on its performance during a recent commissioning run, T-437 at SLAC, which demonstrated charge and position asymmetry precisions of 12 ppb and 2 nm, respectively.

*Submitted to IEEE Transactions on Nuclear Science*

\*Work supported by Department of Energy contract DE-AC03-76SF00515.

# Helicity-Correlated Systematics for SLAC Experiment E158

Peter Mastromarino, T. Brian Humensky, Perry Anthony, Carlos Arroyo, Klejda Bega, Axel Brachmann, Gordon Cates, James Clendenin, Franz-Josef Decker, Ted Fieguth, Emlyn Hughes, G. Mark Jones, Yury Kolomensky, Krishna Kumar, David Relyea, Steve Rock, Owen Saxton, Zen Szalata, Jim Turner, Mike Woods

*Abstract*— Experiment E158 at SLAC will make the first measurement of parity violation in Møller scattering. The left-right cross-section asymmetry in the elastic scattering of a 45 GeV polarized electron beam with unpolarized electrons in a liquid hydrogen target will be measured to an accuracy of better than  $10^{-8}$ , with the expected Standard Model asymmetry being approximately  $10^{-7}$ . Because helicity-correlated (left-right) charge and position asymmetries in the electron beam can give rise to systematic errors in the measurement, great care must be given to beam monitoring and control. We have developed beam current monitors that measure the charge per pulse at the  $3 \times 10^{-5}$  level and RF cavity beam position monitors that measure the position per pulse to  $1 \mu\text{m}$ , which should allow precisions of 1 ppb and 1 nm for the final integrated charge and position asymmetries, respectively. In addition, since most helicity-correlated systematics in the electron beam can be traced back to the laser that drives the photoemission from the GaAs source cathode, we first use careful control of laser beam polarization, point-to-point imaging, and other techniques to minimize systematics. We also provide the capability of modulating in a helicity-correlated way the laser beam's intensity and position as it strikes the photocathode, allowing the implementation of active feedbacks to ensure that the average charge and position asymmetries integrate close to zero over the course of the experiment. We present this system of precision beam monitoring and control and report on its performance during a recent commissioning run, T-437 at SLAC, which demonstrated charge and position asymmetry precisions of 12 ppb and 2 nm, respectively.

*Keywords*— parity violation, polarized electron beam, beam monitoring, beam control

## I. INTRODUCTION

WHILE the weak mixing angle has been precisely measured at the  $Z^0$  pole at CERN and SLAC, additional measurements of similar precision away from the  $Z^0$  pole are needed to look for certain classes of new physics, including additional heavy gauge bosons, contact interactions, electron compositeness, and extra dimensions [1],[2].

K. Bega, E. Hughes, G. Mark Jones, and P. Mastromarino are with the Department of Physics, California Institute of Technology, Pasadena, CA 91125 USA.

T. B. Humensky and D. Relyea are with the Department of Physics, Princeton University, Princeton, NJ 08544 USA.

P. Anthony, A. Brachmann, J. Clendenin, F.-J. Decker, T. Fieguth, S. Rock, O. Saxton, Z. Szalata, J. Turner, and M. Woods are with the Stanford Linear Accelerator Center, Menlo Park, CA 94025 USA.

C. Arroyo and K. Kumar are with the Department of Physics, University of Massachusetts, Amherst, MA 01003 USA.

G. Cates is with the Department of Physics, University of Virginia, Charlottesville, VA 22904 USA.

Yu. Kolomensky is with the Department of Physics, University of California, Berkeley, CA 94720 USA.

Experiment E158 at SLAC will measure the parity violating left-right asymmetry in Møller scattering ( $e^-e^- \rightarrow e^-e^-$ ) at an average  $Q^2$  of  $0.03 (\text{GeV}/c)^2$  to a relative precision of roughly 9%. The raw physics asymmetry, which is directly proportional to the pseudo-scalar weak neutral current coupling  $g_{ee}$  [3], will be approximately 105 ppb (*part per billion*), implying that the combined statistical and systematic errors in the measurement be kept below 10 ppb. This will allow a measurement of the weak mixing angle with a sensitivity of  $\delta(\sin^2(\theta_W)) \approx 0.0008$ , which would be its most precise determination off the  $Z^0$  resonance and provide sensitivity to all of the classes of new physics mentioned above.

At the small angles required by such a low  $Q^2$  measurement of the left-right Møller asymmetry, the scattering cross-section is extremely sensitive to changes in beam position and angle, as can be seen from its leading-order expression:

$$\frac{d\sigma}{d\Omega} = \frac{\alpha^2}{2mE} \frac{(3 + \cos^2 \Theta)}{\sin^4 \Theta} \quad (1)$$

where  $\alpha$  is the fine structure constant,  $E$  is the incident beam energy in the lab frame,  $m$  is the electron mass, and  $\Theta$  is the scattering angle in the center-of-mass frame. Any helicity-correlated differences in beam position or angle at the target could therefore manifest themselves as a left-right scattering rate difference, which in turn could be wrongly interpreted as a physics asymmetry. Such geometric effects can be corrected for, but in order to ensure that the systematic errors stemming from such corrections are kept below the few ppb level, helicity-correlated position and angle differences must be kept below 10 nm and 0.4 nrad, respectively, integrated over the course of the experiment. Likewise it is required that the beam intensity asymmetry averaged for the entire experiment should be no more than 200 ppb. First-order dependence of the Møller asymmetry on the beam intensity asymmetry is partially removed by defining the raw physics asymmetry in terms of detector signals normalized to beam current monitor signals:

$$A_{LR} = \frac{\phi_L/q_L - \phi_R/q_R}{\phi_L/q_L + \phi_R/q_R} \quad (2)$$

where  $\phi_{L(R)}$  is the detector flux signal, and  $q_{L(R)}$  the beam current monitor signal, for a left (right) helicity beam. Such an approach does not work perfectly, however, since detector nonlinearities, which are expected to be 0.5% or better,

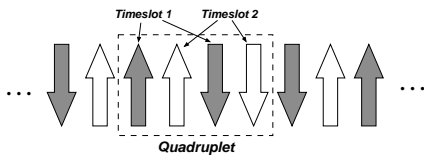


Fig. 1. Example of a valid helicity sequence. The data come in pairs, where the helicity of the second pulse is always the complement of the helicity of the first pulse. Pairs are interleaved to form quadruplets in order to minimize sensitivity to the 60 Hz noise component. Each quadruplet therefore has two timeslots.

will leave some residual dependence on intensity. In addition, beam loading effects, which couple intensity jitter to energy jitter at the 5% level [4], as well as the fact that intensity jitter influences other parameters in the accelerator, motivate keeping the intensity asymmetry below the 200 ppb level.

It is a major challenge of the experiment to keep the helicity-correlated beam parameter differences below the required levels, and an equal challenge to measure these differences with the necessary precision. Doing so requires both high precision beam monitoring devices with which to measure helicity-correlated differences, as well as control devices implemented in feedbacks working to keep those differences small. This paper will describe the beam monitoring and control system employed by E158, reporting on its performance during T-437 at SLAC, a beam test that took place November 1–8, 2000. This test commissioned the necessary precision beam monitoring and control devices, demonstrating significant improvements in performance over earlier studies.

## II. POLARIZED ELECTRON SOURCE

Minimization of helicity-correlated systematics begins at the polarized electron source (PES). The PES consists of two main components: a DC-biased photocathode gun located in the gun vault and a tunable pulsed-laser system located in the source laser room. The two rooms are connected by an approximately 20-m optical transport system (OTS). A strained-layer GaAs crystal is used for the photocathode [5]. When circularly polarized light from the laser (tuned to the band gap of the crystal's active layer) impinges on a GaAs crystal having a properly activated surface, photoexcited electrons escape to vacuum with a circular polarization that is typically 75%. Injection into the linac and acceleration to high energy does not degrade the initial polarization. The laser system employed by E158 is more fully described elsewhere [6], [7]. Here we will discuss some of the key features as they relate to the control of helicity-correlated systematics.

### A. Helicity Determination

In order to carry out the measurement of the parity violating left-right asymmetry in Møller scattering, it is necessary to be able to alternate the helicity of the SLAC electron beam on a pulse-to-pulse basis. Flipping rapidly between helicity states minimizes the experiment's sensitivity to slow drifts, an essential first step in the control of

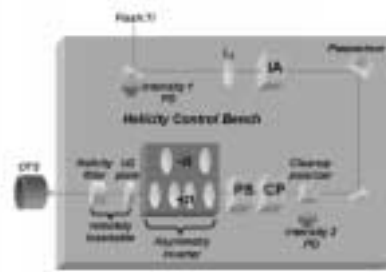


Fig. 2. Diagram of the source optics setup. The CP and PS Pockels cells provide circular polarization of better than 99.8%. The IA cell and piezomirror implement the intensity asymmetry and position difference feedback loops, respectively.

helicity-correlated systematics. The helicity of the beam is actually determined in a pair-wise pseudo-random manner, as illustrated in Fig. 1. Each helicity pair is interleaved with another pair, forming a helicity quadruplet. Since the beam repetition rate for E158 will be 120 Hz, interleaving pairs in this way is necessary in order to avoid the large noise component at 60 Hz. The two pairs comprising each quadruplet are referred to as timeslots, as is shown in the figure. This procedure just determines the helicity sequence. The actual polarization takes place in the source laser room, on the helicity control bench. Here great care must be taken in order to ensure that any helicity correlations induced during the polarization process are minimized.

### B. Helicity Control Bench

All of the optics associated with circular polarization and the control of helicity correlations are housed on the helicity control bench, shown in Fig. 2. The laser light entering the bench is generated by a flash lamp-pumped Ti:sapphire rod [8] at the beam repetition rate of the linac. A 370 ns pulse is sliced from the laser output by the pulse-shaping optics (located on a bench not shown), a combination of crossed linear polarizers and a Pockels cell supplied with a pulse of high voltage. The lens  $L_3$  is the last of a triplet designed to control beam size and divergence at the polarization Pockels cells. The IA Pockels cell implements the intensity asymmetry (or IA) feedback loop, which will be discussed in Sec. III, by introducing a helicity-correlated rotation to the laser's linear polarization. The cleanup polarizer, oriented so as to only transmit horizontally polarized light, then transforms this into the requisite intensity asymmetry correction. The piezomirror is a mirror mounted on a piezo stack whose movement can be controlled on a pulse-by-pulse basis, inducing helicity-correlated position differences as part of the position (or POS) feedback loop.

The Circular Polarization (CP) and Phase Shift (PS) Pockels cells (Cleveland Crystals QX2035) are used to generate nearly perfect circular polarization at the cathode. For each helicity pair, these Pockels cells' left- and right-

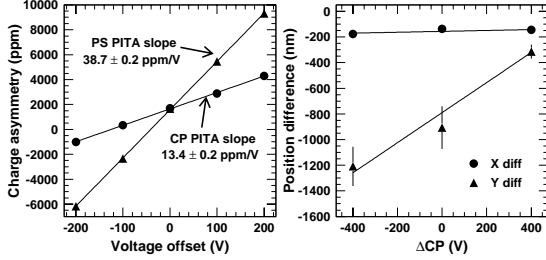


Fig. 3. Helicity-correlated phase shifts in the optical transport system, coupled with the 10% analyzing power of the photocathode, produce dependencies of the charge and position asymmetries on the CP and PS cell voltages.

pulse voltages are set in the following manner:

$$\begin{aligned}
 V_L^{CP} &= -V_{QW} + \delta_L^{CP} + \Delta^{CP} \\
 V_R^{CP} &= +V_{QW} + \delta_R^{CP} + \Delta^{CP} \\
 V_L^{PS} &= \delta_L^{PS} + \Delta^{PS} \\
 V_R^{PS} &= \delta_R^{PS} + \Delta^{PS}
 \end{aligned}
 \tag{3}$$

where  $V_{QW}$  is the voltage (approximately 2800 V) at which the Pockels cells act as quarter-wave plates, and the other voltages denoted by  $\delta$  are small but necessary perturbations that compensate for imperfections in the cells' alignments. The CP cell's fast axis is oriented at  $45^\circ$  from the vertical, so that pulsing it at  $\pm V_{QW}$  should ideally produce circularly polarized light of either helicity. The PS cell's fast axis is vertical. We require that  $|\delta_L^{CP} - \delta_R^{CP}| < 100$  V, and similarly for the PS cell. The quarter-wave voltage  $V_{QW}$  and the perturbation voltages discussed above are determined by fitting the data obtained from cell voltage scans with the helicity filter inserted into the path of the laser beam to transmission and extinction curves. The helicity filter is a quarter-wave plate glued to a linear polarizer such that circular polarization of one helicity is transmitted while the other is extinguished. The voltages are varied as free parameters, resulting in transmission to extinction ratios better than 1000:1, implying at least 99.8% circular polarization. If the fits yield perturbation voltages that fail to satisfy the criteria given above, the Pockels cells' alignments are adjusted according to certain specified procedures and the scans are performed again.

### C. PITA Slopes and Position Effects

The other voltages in (3),  $\Delta^{CP}$  and  $\Delta^{PS}$ , are used to adjust the size of the intensity asymmetry in the electron beam, caused by helicity-correlated phase shifts encountered in the OTS that induce linear polarization at the cathode. The analyzing power of the photocathode, which is roughly 10%, transforms this linear polarization into an intensity asymmetry [9]. This asymmetry is referred to as the PITA (Polarization Induced Transport Asymmetry) effect, and the voltages  $\Delta^{CP}$  and  $\Delta^{PS}$  turn out to be directly proportional to the size of the asymmetry [10]. This sensitivity is shown graphically in Fig. 3. We carefully tune

these voltages so that the intensity asymmetry is nulled to the  $10^{-4}$  level, thereby reducing the size of the corrections the IA loop needs to make. In addition, left-right electron beam position differences were found to correlate with both these voltages. In Fig. 3 we show the response of left-right position differences to  $\Delta^{CP}$  variations, while  $\Delta^{PS}$  was simultaneously varied to null the charge asymmetry. While the physical origin of this sensitivity is not well understood, it certainly proves useful as an additional means of minimizing helicity-correlated systematics.

Both the CP and PS Pockels cells possess some residual birefringence that depends on position across the face of the crystal. Consequently, the position at which the laser beam passes through the crystals can have an effect on the helicity-correlated position differences in the electron beam. For this reason both Pockels cells were mounted on  $x$ - $y$  translation stages, which were used to control the laser's path through the crystals. This gives another method by which to minimize left-right position differences. Studies have indicated that the Pockels cells can also act as helicity-correlated lenses, making point-to-point imaging from the CP cell to the cathode desirable. Such imaging minimizes the contribution of any helicity-correlated steering from the CP cell. In practice, the PS cell is imaged, leaving an effective lever arm of approximately 15 cm from the CP cell to the cathode, a significant reduction from the 25 m actual distance between the CP cell and cathode. This image point produces an effective lever arm of approximately 50 cm for the piezomirror, giving the piezomirror a dynamic range of 50–60  $\mu\text{m}$  at the cathode. In addition, designing the waist of the beam to be near the CP and PS cells minimizes the sensitivity to the position-dependent birefringence mentioned above. However, having the beam well collimated through the Pockels cells is essential, so the focus must be a gentle one. We found the optimum beam sigma to be approximately 1 mm at the CP cell.

### D. Systematics Cancellation Optics

The two devices immediately downstream of the PS cell are optics designed to provide slow (i.e., *not* pulse-to-pulse) cancellation of helicity-correlated systematics. The first device is called the asymmetry inverter. It is composed of two separate lens configurations, a lens doublet and a lens quadruplet, mounted on a translation stage. The lens doublet acts as a telescope providing a magnification of -2.25. The lens quadruplet also acts as a telescope, but provides a magnification of +2.25. The stage can be moved such that the laser light passes through either lens configuration, allowing a transformation of  $\pm 2.25I$  to be applied to the beam. Switching between the two states of the asymmetry inverter, by inverting both the spatial distribution of the beam's intensity profile and its angle leaving the helicity control optics, should therefore yield at least a partial cancellation of systematic effects caused by helicity-correlated beam fluctuations. The second systematics cancellation device on the helicity control bench is the remotely insertable half-wave plate. Insertion of the half-wave plate provides a way of slowly reversing the helicity of the beam, while leav-

ing all other aspects of the experiment untouched. This can provide cancellation of certain classes of helicity-correlated systematics, for instance false asymmetries caused by electronic crosstalk and voltage-induced Pockels cell steering. It can also provide convincing evidence for parity-violating physics, as the sign of the physics asymmetry will correlate with the presence of the half-wave plate in the path of the laser beam. In addition, the half-wave plate can provide partial cancellation of systematics deriving from residual linear polarization in the laser beam, the degree of cancellation depending on the half-wave plate's orientation relative to the polarization direction.

### E. Cathode Diagnostics Bench

After leaving the helicity control bench, the laser beam traverses the 20 m through the OTS to the gun vault. The cathode diagnostics bench lies immediately before the entrance to the gun and houses optics that control the final size and position of the beam and monitor various aspects of the cathode's performance. These optics are described in more detail in [7]. In addition, this bench houses an additional half-wave plate that can be used in a similar manner as the one on the helicity control bench to control helicity-correlated systematics. From the cathode diagnostics bench the laser beam is directed to the gun photocathode. The cathode bias is typically  $-120$  kV. As previously mentioned, the laser pulse length is on the order of hundreds of nanoseconds. The electron beam temporal pulse shape follows the laser pulse shape at low optical energies, but is typically distorted at high optical energies, such as those required for T-437, by the surface charge limit (SCL) [11] of the GaAs crystal. RF bunching is used to define the micropulse structure. After injection, the beam is accelerated to an energy of 1.2 GeV in the linac before entering the test stand housing the beam monitoring devices being commissioned as part of T-437.

## III. SOURCE FEEDBACKS

Besides commissioning the new readout electronics associated with the beam monitoring devices described in Sec. IV, an important goal of beam test T-437 was to demonstrate that helicity-correlated asymmetries in the electron beam could be reduced to the 200 ppb level for intensity and the 10 nm level for position. The techniques described in the previous sections typically succeed in reducing the charge asymmetry to the 100 ppm level and the position differences to the 1  $\mu\text{m}$  level. In order to achieve the two orders of magnitude in further reduction of these systematics, active feedbacks are required. The implementation of these feedbacks in the source optics system was described in Sec. II-B. We now describe the basic operating principle behind the feedbacks, at the same time highlighting an important side benefit of their usage, namely faster-than-statistical convergence of helicity-correlated systematics.

### A. Basic Feedback Algorithm

Both the intensity and position feedback loops operate by the same principle: average beam asymmetries for a given number of pairs, then induce an asymmetry on the beam chosen to compensate for the observed asymmetry. The basic algorithm is thus:

$$\begin{aligned} A_{induced}^1 &= 0 \\ &\vdots \\ A_{induced}^i &= A_{induced}^{i-1} - A_{observed}^{i-1} \end{aligned} \quad (4)$$

where

$$A_{observed}^i = A_{induced}^i + A_{beam}^i + A_{statistics}^i \quad (5)$$

Here  $i$  denotes the number of measurements. By following this basic prescription, two benefits are received. First, the average asymmetry approaches zero, and second, it approaches zero at a faster-than-statistical rate. One can see this by noticing that in (4), random, uncorrelated beam asymmetry errors become perfectly correlated — to the extent that beam measuring device resolution is negligible compared to the average statistical fluctuations of a single measurement. With the exception of the last asymmetry measurement, all of the measurements' statistical fluctuations (denoted in (5) by  $A_{statistics}^i$ ) have been arranged to cancel one another. Therefore only one error bar enters into the error propagation formula when the average of the measurements is computed. In this way, purely statistical  $1/\sqrt{N}$  scaling (where  $N$  is the total number of asymmetry measurements) becomes seemingly improbable  $1/N$  scaling. We investigate this feature below as it relates to meeting our goals for the helicity-correlated intensity and position systematics.

### B. Intensity Asymmetry Feedback

In order to keep its contribution to the final systematic error on the physics asymmetry at the ppb level, the intensity asymmetry integrated over the course of the experiment needs to remain below 200 ppb, given the expected 0.5% detector and toroid combined nonlinearities. For each helicity pair, the intensity asymmetry  $A_I$  is given by:

$$A_I = \frac{q_L - q_R}{q_L + q_R} \quad (6)$$

If the pulse-to-pulse electron beam intensity jitter is defined to be  $\delta I_{pp}$ , and the final physics data set is projected to consist of 200 million pairs, this puts an upper limit on  $\delta I_{pp}$  of approximately:

$$\begin{aligned} (\delta I_{pp})_{max} &= \sqrt{2} \cdot \sqrt{2 \times 10^8} \cdot 200 \text{ ppb} \\ &= 0.4\% \end{aligned} \quad (7)$$

where the  $\sqrt{2}$  in front comes from the fact that we follow the difference-over-sum convention for defining the asymmetry in (6). If the pulse-to-pulse intensity jitter were any larger than this upper limit, the intensity asymmetry would

not be known with sufficient statistical precision to achieve our goal of 200 ppb integrated for the experiment. Intensity jitter this small is hard to achieve in practice. Therefore, an intensity asymmetry feedback is needed in order to yield a factor of ten improvement over statistical scaling, allowing the maximum permissible intensity jitter to rise from 0.4% to 4%.

### C. Position Differences Feedbacks

In order to keep their contributions to the final systematic error on the physics asymmetry at the ppb level, helicity-correlated position differences integrated over the entire experiment need to remain below 10 nm. For each helicity pair, we define a position difference  $\Delta_x$  to be:

$$\Delta_x = x_L - x_R \quad (8)$$

and similarly for  $y$ . If the pulse-to-pulse electron beam position jitter is defined to be  $\delta x_{pp}$ , a calculation analogous to (7) finds an upper limit on  $\delta x_{pp}$  of approximately:

$$\begin{aligned} (\delta x_{pp})_{max} &= (1/\sqrt{2}) \cdot \sqrt{2 \times 10^8} \cdot 10 \text{ nm} \\ &= 100 \mu\text{m} \end{aligned} \quad (9)$$

where the  $1/\sqrt{2}$  in front comes from our definition of the position difference in (8). This limit is usually not exceeded by the electron beam, whose position jitter is typically on the order of tens of micrometers. Consequently, the super-statistical scaling produced by the position feedback is not strictly required.

## IV. BEAM MONITORING DEVICES

An important part of T-437 was to commission new, high-precision readout electronics for beam monitoring devices, demonstrating their resolutions to meet or exceed the requirements put forth in the E158 proposal. We commissioned electronics for two types of devices: toroids, which monitor beam charge, and beam position monitors (or *BPM's*), which, as their name implies, monitor beam position. Each toroid is the inductance in an RLC circuit, so that the electron beam passing through it generates a ringing signal that is rectified and integrated, using custom-built 16-bit ADC's. The BPM's each have three copper cavities possessing characteristic resonant frequencies of 2856 MHz. The BPM's are therefore known as RF cavity beam position monitors. The cavities are used to measure charge,  $x$  position, and  $y$  position, and are thus called  $Q$ ,  $X$ , and  $Y$  cavities, respectively. As the electron beam passes through the BPM, each cavity produces a signal that is fed into a processor unit that finds the "real" and "imaginary" amplitudes of the signal, where the "real" part is defined to be in phase with a local oscillator (LO) signal, and the "imaginary" part  $90^\circ$  out of phase. The LO signal is produced by sending a 476 MHz signal from the linac into a  $6\times$  frequency multiplier. As the position of the electron beam changes, the amplitude of the RF signal it generates also changes. For small deviations from the cavity's center, the RF signal has a linear dependence on

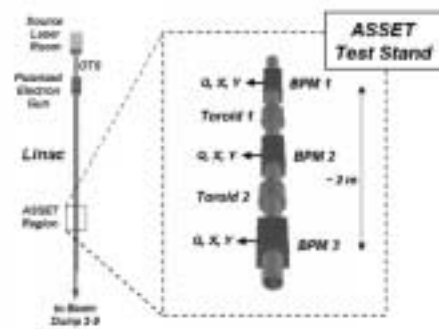


Fig. 4. Test stand in the 1.2 GeV ASSET region. Beam test T-437 commissioned two toroids and three BPM's.

position. The size of the RF signal can be translated into physical position information once calibrations have been performed against devices whose calibrations are already known. All BPM signals are also fed into custom-built 16-bit ADC's.

### A. Device Resolution Requirements

The resolution required of the toroids is determined by the 1 ppb precision needed on the final intensity integrated asymmetry measurement. Allowing for a projected data set consisting of 200 million pairs, the resolution  $\sigma_{toroid}$  of a single pulse-to-pulse measurement of the beam charge must be better than the following upper limit:

$$(\sigma_{toroid})_{max} = \sqrt{2} \cdot \sqrt{2 \times 10^8} \cdot 1 \text{ ppb} = 20 \text{ ppm} \quad (10)$$

where the factor of  $\sqrt{2}$  in front follows from the difference-over-sum convention used in (6) for defining the intensity asymmetry. Likewise, the BPM resolution goal is roughly  $1 \mu\text{m}$ . While this level of resolution may be more than necessary, it is desirable to have the resolution be as good (i.e., as low) as possible. In addition, this resolution should ensure that the systematic error contributions stemming from corrections of position-related false asymmetries remain at the ppb level, even given the partial breakdown of some assumptions related to detector performance.

Beam test T-437 commissioned three BPM's and two toroids, housed on a test stand, shown in Fig. 4, located in what is known as the ASSET region. The ASSET region is in Sector 2-3 of the linac, at which point the electrons have been accelerated to 1.2 GeV. The beam pulse consisted of  $2.3 \times 10^{11}$  electrons in 370 ns. The beam rate was 59 Hz, with 1 Hz of pedestal (no-beam) data. The beam was dumped in Sector 2-9, 60 m downstream of ASSET. As Fig. 4 shows, the toroids and BPM's are grouped closely together, allowing their resolutions to be tested by comparing measurements taken from neighboring devices. This testing procedure will be fully described in Sec. VI.

## V. DATA ACQUISITION SYSTEM

The data acquisition (DAQ) system employed by the E158 experiment, and commissioned during the T-437 beam test, included custom-built 16-bit ADC's, as mentioned in the previous section. The core system components, along with data paths, are shown schematically in

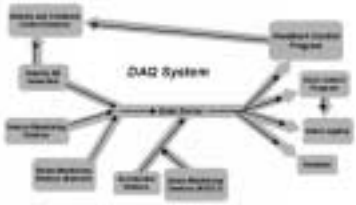


Fig. 5. The DAQ system used for beam test T-437 at SLAC. The feedback control received beam monitoring data and remotely controlled the hardware at the source.

Fig. 5. All communications among these components occurred via TCP/IP networking, with fiber optic cable being used for the longer connections. The data server supplied the data from the various monitoring devices at the source, in the injector region, and in ASSET. The feedback control program, run from a terminal in the End Station A (ESA) Counting House, located approximately two miles from the source and injector region, processed the data from the server in real time and calculated the asymmetries that needed to be applied to control systematics. The combination of voltages capable of inducing these asymmetries was sent, along with the helicity data from the helicity bit generator, via the accelerator's broadband communications network to receivers located in ASSET and the counting house. The helicity bit generator implemented a pseudo-random bit generator algorithm described in [12]. The data logging program was used to log the data stream to a disk file which was subsequently staged to tape. The DAQ control program controlled the beginning and ending of runs, and the logging, as well as providing some basic monitoring functions. Various analysis programs generated ntuples from the raw data for concurrent processing. Such a distribution of data acquisition and control over the length of the SLAC accelerator is fairly unique.

## VI. RESULTS

The results of the T-437 beam test naturally divide into three categories: device resolution and asymmetry agreement, feedback performance, and systematics inversion tests. Results from each of these categories will be presented and compared to the best results from previous studies.

### A. Device Resolution and Asymmetry Agreement

In Fig. 6 we show an example of the procedure used to compute toroid resolution and probe intensity asymmetry agreement. The asymmetry measurement  $A_2$  of the second toroid is plotted against the asymmetry measurement  $A_1$  of the first toroid, and a least-squares minimization fit is performed to find the slope  $m$  of the resulting line (which gives information on toroid linearity). The toroid resolution per pulse is given by:

$$\sigma_{toroid} = \sqrt{2} \times \text{RMS of } (A_2 - m \cdot A_1) \quad (11)$$

The asymmetry agreement is the mean of the same distribution. Fig. 6 shows charge resolution and agreement results for a typical sample of data, demonstrating toroid

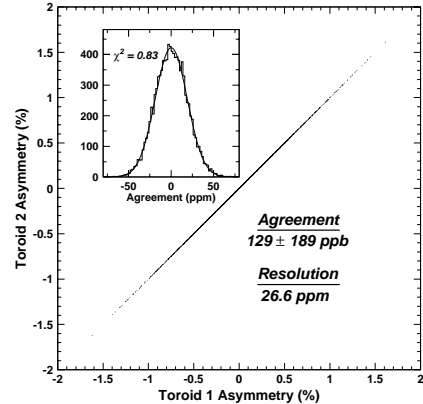


Fig. 6. Toroid asymmetry agreement for a small sample of the T-437 data set. The asymmetry from one toroid is plotted against the asymmetry from the other (where beam jitter is responsible for the spread in the data), and the residuals are plotted and fit to a gaussian function. Toroid resolution is less than 30 ppm.

resolution of less than 30 ppm. The dominant source of noise limiting this resolution was electronic, which will fall off as a fraction of the signal as we go to higher current and the full dynamic range of the ADC's is exploited. Hence, at the full current requested by E158 ( $6 \times 10^{11}$  e<sup>-</sup> per pulse), the resolution is expected to improve by about a factor of two. This will bring the resolution below the upper limit found in (10), and would thus allow a determination of the final integrated intensity asymmetry at the 1 ppb level. BPM resolution and agreement are computed in an entirely analogous manner. We use the first and last BPM's to predict what the position should be at the middle BPM. We define  $\Delta_1$ ,  $\Delta_2$ , and  $\Delta_3$  to be the left-right position differences as measured by BPM's 1, 2, and 3, respectively. We plot  $(\Delta_1 + \Delta_3) / 2$  versus  $\Delta_2$ , and perform a least-squares minimization fit to find the slope  $m$  of the resulting line.

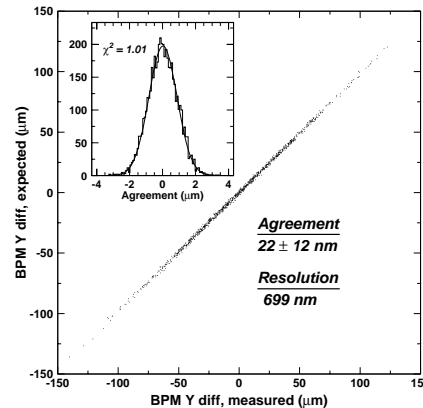


Fig. 7. Position difference agreement for a small sample of the T-437 data set. The first and last BPM's are used to predict what the position difference should be at the middle BPM. Beam jitter is responsible for the spread in the data. The residuals are plotted and fit to a gaussian function. BPM  $y$  resolution is seen to be less than 700 nm.

TABLE I  
GOALS AND RESULTS FOR T-437.

	<i>Achieved in GTL</i>	<i>T-437 Goal</i>	<i>E158 Goal</i>	<i>Achieved in T-437</i>
Intensity Asymmetry Agreement	200 ppb	200 ppb	200 ppb	$1/\sqrt{N}$ $0.2 \pm 5.7$ ppm $1/N$ $190 \pm 330$ ppb
Intensity Asymmetry Agreement	1 ppm	10 ppb	1 ppb	$6 \pm 12$ ppb
Position Difference	5 nm	10 nm	10 nm	$\begin{cases} x: -6 \pm 37 \text{ nm} \\ y: -19 \pm 49 \text{ nm} \end{cases}$
Position Difference Agreement	100 nm	1 nm	1 nm	$\begin{cases} x: -6 \pm 6 \text{ nm} \\ y: -19 \pm 8 \text{ nm} \end{cases}$ $\begin{cases} x: -1.4 \pm 0.9 \text{ nm} \\ y: -4.2 \pm 1.8 \text{ nm} \end{cases}$

The resolution  $\sigma_{bpm}$  is then equal to:

$$\sigma_{bpm} = \frac{2}{\sqrt{6}} \times \text{RMS of } \left\{ \frac{\Delta_1 + \Delta_3}{2} - m \cdot \Delta_2 \right\} \quad (12)$$

This procedure eliminates common mode beam jitter from our definition of  $\sigma_{bpm}$ , leaving only the random noise inherent in the readout electronics. The BPM agreement is the mean of the same distribution. The  $x$  and  $y$  BPM resolutions were demonstrated to be 900 nm and 700 nm, respectively, exceeding our goal of 1  $\mu\text{m}$ . Fig. 7 shows BPM resolution and agreement results for a typical sample of data.

Table I summarizes the asymmetry agreement results for T-437, comparing them to goals that were determined by considering the statistics that could be reasonably achieved in a week of running. In addition, the table compares the results to the final goals required by E158 and to the best previous results from studies carried out in the gun test lab (GTL), a facility consisting of a duplicate of the polarized electron gun and the first few meters of the electron beamline, terminating in a Faraday cup. The agreement numbers for the toroids and BPM's commissioned during T-437 show two orders of magnitude in improvement over the GTL results.

### B. Integrated Asymmetries and Differences

In Fig. 8 we show the intensity asymmetry and the  $x$  and  $y$  position differences converging to zero under the control of the IA and POS feedback loops. Asymmetry calculations were performed by dividing the data into  $N$  blocks called *miniruns*. For the intensity asymmetry feedback loop, a minirun consisted of 2000 pulse pairs, while for the position difference feedback loop, a minirun consisted of 10,000 pulse pairs. Dividing the data into miniruns is necessary in order to average out statistical fluctuations in the beam asymmetries, since the feedback control devices have finite dynamic ranges. The intensity asymmetry loop monitored toroid 1 in order to calculate its corrections, while the position loop monitored BPM 2. The smooth curves in each

of the plots contained in Fig. 8 show how the error bars would scale given statistical  $1/\sqrt{N}$ -type evolution. In all cases, the helicity-correlated differences are seen to converge to zero faster than normal statistics would allow, as is expected for an active feedback system. The figure contains data representing several long feedback runs, each consisting of a few hours of continuous data taken under constant conditions. Table I summarizes the final results from these and other feedback runs for the integrated intensity asymmetry and position differences. The error bars quoted are for normal statistical scaling. However, as the data in Fig. 8 clearly show, the true errors on the final integrated asymmetries are much smaller than normal statistics would predict. Therefore, Table I includes error bars calculated using both  $1/\sqrt{N}$  and  $1/N$  statistical scaling. While the results are all consistent with zero, they fall just short of meeting the specified goals due to a lack of statistical power.

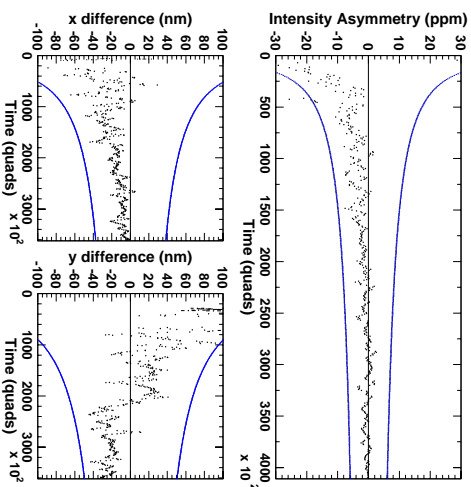


Fig. 8. This plot shows time histories for the integrated charge asymmetry and the integrated  $x$  and  $y$  position differences, as measured by the devices in ASSET1, while both source feedback loops were running.

TABLE II  
ASYMMETRY INVERTER RESULTS.

<i>Induced Feedback Correction</i>	<i>-2I State</i>	<i>+2I State</i>	<i>Average</i>
X Position	$262 \pm 48$ nm	$-39 \pm 71$ nm	$168 \pm 40$ nm
Y Position	$-862 \pm 109$ nm	$1157 \pm 130$ nm	$-29 \pm 84$ nm
Intensity	$-281 \pm 20$ ppm	$78 \pm 29$ ppm	$-165 \pm 16$ ppm

TABLE III  
HALF-WAVE PLATE RESULTS.

<i>Asymmetry</i>	<i><math>\lambda/2</math> In</i>	<i><math>\lambda/2</math> Out</i>	<i>Average</i>
BPM2 <i>x</i>	$126 \pm 12$ nm	$119 \pm 11$ nm	$-7 \pm 8$ nm
BPM2 <i>y</i>	$-1732 \pm 57$ nm	$-581 \pm 51$	$-461 \pm 38$ nm
Toroid 1	$-1.5 \pm 5.1$ ppm	$-14.7 \pm 4.7$ ppm	$7.2 \pm 3.5$ ppm

### C. Systematics Inversions

Even though in theory a feedback will null a helicity-correlated systematic given a sufficient length of time, no matter how large its initial size, it is desirable to have the systematic itself average as close to zero as possible over the course of the experiment. Alternating the state of the asymmetry inverter should partially cancel any residual position or intensity systematics not nulled by the feedbacks, and in addition average the corrections induced by the feedbacks to zero. During the feedback runs whose results are given in Table I, the state of the asymmetry inverter was flipped once. Table II lists the position and intensity corrections induced by the feedbacks while the asymmetry inverter was in either state. We see a substantial cancellation of the large *y* corrections, indicating that the asymmetry inverter was indeed providing some cancellation of systematics. Inserting a half-wave plate into the path of the laser beam at the source provides a powerful means of separating false asymmetries like those caused by Pockels cell steering effects and electronic crosstalk from actual physics asymmetries. Table III summarizes what effect insertion of the half-wave plate on the helicity control bench had on charge and position systematics. During the time these data were being taken, only the intensity asymmetry feedback loop was running, using a toroid in the injector region instead of in ASSET as its measuring device. We observe considerable cancellation of helicity-correlated charge and position systematics.

## VII. CONCLUSIONS

Overall, the system of precision beam monitoring and control outlined in this paper performed admirably during beam test T-437 at SLAC, zeroing the average charge asymmetry to within 330 ppb and the average position differences to within 20 nm. Additionally, it demonstrated a

hundred-times improvement over earlier studies in its level of precision, maintaining agreement between toroids to within 12 ppb and agreement between BPM's to within 2 nm. While these achievements fall just short of meeting the specified goals, they all appear to be statistics-limited. Future running should therefore see all of the E158 goals outlined in Table I met. As indicated in Table II, typical corrections were on the order of 100 ppm for the intensity asymmetry loop and 1  $\mu$ m for the position difference loop, implying that the source feedbacks provide a factor of 100–1000 reduction in the sizes of the helicity-correlated systematics. This remarkable degree of cancellation is necessary in order to satisfy the stringent requirements imposed by a precise determination of the weak mixing angle at low energy.

## REFERENCES

- [1] A. Czarnecki and W. J. Marciano, Phys. Rev. D **53**, 1066 (1996).
- [2] A. Czarnecki and W. J. Marciano, Int. J. Mod. Phys. A **15**, 2365 (2000).
- [3] E. Derman and W. J. Marciano, Ann. Phys. **121**, 147 (1979).
- [4] F.-J. Decker, Z. D. Farkas, J. Turner, SLAC preprint SLAC-PUB-8113 (1999).
- [5] T. Maruyama, E. L. Garwin, R. Prepost, G. H. Zapalac, Phys. Rev. B **46**, 4261 (1992).
- [6] R. Alley, H. Aoyagi, J. Clendenin, J. Frisch, C. Garden, E. Hoyt, et al., Nucl. Inst. Meth. A **365**, 1 (1995).
- [7] T. B. Humensky, R. Alley, A. Brachmann, M. Browne, G. D. Cates, J. Clendenin, et al., *Laser and Beam Control Technologies*, SPIE Conference, to be submitted (2002).
- [8] K. Witte, SLAC preprint SLAC-PUB-6443 (1994).
- [9] R.A. Mair, R. Prepost, H. Tang, E. L. Garwin, T. Maruyama, and G. Mulhollan, Phys. Lett. A **212**, 231 (1996).
- [10] G. D. Cates et al., Nucl. Inst. Meth. A **278**, 293 (1989).
- [11] M. Woods, J. Clendenin, J. Frisch, A. Kulikov, P. Saez, D. Schultz, et al., J. Appl. Phys. **73**, 8531 (1993).
- [12] P. Horowitz and W. Hill, *The Art of Electronics*, pp. 437–442, Cambridge University Press, Cambridge (1980).